

**Microscopic origin of wall slip during flow of an entangled DNA solution in microfluidics
Flow induced chain stretching versus chain desorption**

Hemminger, Orin; Boukany, Pouyan E.

DOI

[10.1063/1.4991496](https://doi.org/10.1063/1.4991496)

Publication date

2017

Document Version

Final published version

Published in

Biomicrofluidics

Citation (APA)

Hemminger, O., & Boukany, P. E. (2017). Microscopic origin of wall slip during flow of an entangled DNA solution in microfluidics: Flow induced chain stretching versus chain desorption. *Biomicrofluidics*, 11(4), Article 044118. <https://doi.org/10.1063/1.4991496>

Important note

To cite this publication, please use the final published version (if applicable).
Please check the document version above.

Copyright

Other than for strictly personal use, it is not permitted to download, forward or distribute the text or part of it, without the consent of the author(s) and/or copyright holder(s), unless the work is under an open content license such as Creative Commons.

Takedown policy

Please contact us and provide details if you believe this document breaches copyrights.
We will remove access to the work immediately and investigate your claim.

Microscopic origin of wall slip during flow of an entangled DNA solution in microfluidics: Flow induced chain stretching versus chain desorption

Orin Hemminger, and Pouyan E. Boukany

Citation: *Biomicrofluidics* **11**, 044118 (2017);

View online: <https://doi.org/10.1063/1.4991496>

View Table of Contents: <http://aip.scitation.org/toc/bmf/11/4>

Published by the [American Institute of Physics](#)

Articles you may be interested in

[Electrophoretic stretching and imaging of single native chromatin fibers in nanoslits](#)

Biomicrofluidics **11**, 044108 (2017); 10.1063/1.4996340

[Generating 2-dimensional concentration gradients of biomolecules using a simple microfluidic design](#)

Biomicrofluidics **11**, 044111 (2017); 10.1063/1.4991550

[Rapid, chemical-free breaking of microfluidic emulsions with a hand-held antistatic gun](#)

Biomicrofluidics **11**, 044107 (2017); 10.1063/1.4995479

[The role of shear stress and altered tissue properties on endothelial to mesenchymal transformation and tumor-endothelial cell interaction](#)

Biomicrofluidics **11**, 044104 (2017); 10.1063/1.4991738

[Rapid evaporation-driven chemical pre-concentration and separation on paper](#)

Biomicrofluidics **11**, 044116 (2017); 10.1063/1.4989627

[A simple and reusable bilayer membrane-based microfluidic device for the study of gradient-mediated bacterial behaviors](#)

Biomicrofluidics **11**, 044114 (2017); 10.1063/1.4993438

Looking for a specific instrument?



Easy access to the latest equipment.
Shop the *Physics Today* Buyer's Guide.

PHYSICS TODAY

lasers imaging
VACUUM EQUIPMENT instrumentation
software MATERIALS
cryogenics + MORE...

Microscopic origin of wall slip during flow of an entangled DNA solution in microfluidics: Flow induced chain stretching versus chain desorption

Orin Hemminger^{a)} and Pouyan E. Boukany^{b)}

Department of Chemical Engineering, Delft University of Technology, Delft, The Netherlands

(Received 21 June 2017; accepted 21 August 2017; published online 31 August 2017)

Despite the relevance and importance of slip, a fundamental understanding of the underlying molecular mechanisms of wall slip in polymer flow is still missing. In this work, we investigate the slip behavior of an entangled DNA solution at a molecular scale using a confocal microscope coupled to a microfluidic device. From microscopic measurement, we obtain both the velocity profile and conformation of polymeric chains by visualizing DNA molecules during flow on various surfaces (ranging from weak to strong interactions with DNA molecules). In channel flow at a low Weissenberg number ($Wi = 0.14$), we observe a parabolic flow for an APTES-treated glass (with strong interaction with DNA) in the absence of slip, while a significant amount of slip has been observed for a regular glass (with a weak interaction with DNA). At higher flow rates ($Wi > 1.0$), strong slip appears during flow on APTES-treated surfaces. In this case, only immobile DNA molecules are stretched on the surface and other bulk chains remain coiled. This observation suggests that the flow induced chain stretching at the interface is the main mechanism of slip during flow on strong surfaces. Conversely, for slip flow on surfaces with weak interactions (such as unmodified or acrylate-modified glasses), polymeric chains are desorbed from the surface and a thin layer of water is present near the surface, which induces an effective slip during flow. By imaging DNA conformations during both channel and shear flows on different surfaces, we elucidate that either chain desorption or flow-induced stretching of adsorbed chains occurs depending on the surface condition. In general, we expect that these new insights into the slip phenomenon will be useful for studying the biological flow involving single DNA molecule experiments in micro/nanofluidic devices. *Published by AIP Publishing.* [<http://dx.doi.org/10.1063/1.4991496>]

I. INTRODUCTION

The ability to control the dynamics of biopolymers (such as DNA molecules, actin filaments, and microtubules) in microfluidic devices, where geometry and intrinsic fluid length scales become comparable, is of fundamental and practical interest in both biophysics and molecular biology.^{1,2} Most biological fluids are viscoelastic and have a complex rheological response to fast flow and deformation. One key question concerns the nature of the boundary condition of biological fluids at solid surfaces during fast flow. One of the simplest boundary conditions is the no-slip boundary condition, where it assumes no relative motion between the fluid and the solid substrate at the boundary. This empirical no-slip boundary condition was traditionally applied for many types of problems in fluid mechanics because it has been validated for the flow of ordinary Newtonian fluids at the macroscopic scale.^{3,4} However, as the characteristic length scale of the flow devices decreases, there has been a debate on this boundary

^{a)}Department of Chemical and Biomolecular Engineering, The Ohio State University, Columbus, Ohio 43210, USA.

^{b)}Electronic mail: P.E.Boukany@tudelft.nl.

condition.^{5–8} In particular, it is widely accepted that several types of complex fluids such as polymeric melts and solutions,^{9–12} elastomers,¹³ gels,¹⁴ wormlike micelles,^{15–17} foams,^{18,19} emulsions,²⁰ and colloidal suspensions^{21,22} slip over a solid substrate when the wall shear stress (or shear rate) exceeds a critical value. The wall slip has a paramount effect on the flow and deformation of these complex fluids. So far, not much is known about the microscopic origins of slip in these fluids. A full understanding of the molecular nature of slip is required to control processes in which complex flows play a role.²³

The entangled polymeric fluids provide perhaps the richest examples of the wall slip phenomenon among complex fluids^{9,12} due to its wide practical applications in many fields such as coating,^{24,25} polymer enhanced oil recovery,^{26–30} mixing and extrusion,³¹ lubrication in industrial or biological systems,^{32,33} and lab-on-chip technologies.^{2,34–37} Many of these processes encountered in nature and industry involve the interaction of macromolecules with different surface environments (wall). Despite the relevance and importance of wall slip in polymer flow, the molecular mechanisms of wall slip remain poorly understood.²³ Both the microstructure and the origin of wall slip can vary significantly depending upon the nature of the interaction between the polymer chain and the solid surface. The main objective of this work is to fundamentally address the molecular mechanisms of slip of the entangled polymer at different surface conditions (with strong and weak interactions) in the strong flow regime.

Depending on the application, wall slip can be either favourable or deleterious. In polymer processing and micro/nano-fluidics, wall slip can be beneficial and economically viable because (i) it reduces the required force/pressure to transport polymeric fluids in flow devices (in particular for pressure driven transport in nanofluidics),^{9,38,39} (ii) it optimizes the liquid transport by electro-osmotic flow in micro/nano-fluidic systems,^{39,40} (iii) it forms a thin layer of high shear zone next to the wall surface, which can align and stretch tethered chains for molecular electronics and sensing applications,^{37,41} and (iv) it postpones the shark-skin and melt fracture during extrusion to higher flow rates, which allows the production of smoother and glossier polymeric products.^{9,38} However, slip is always detrimental during rheometric measurements because it leads to large errors and flow discontinuity across the sample thickness due to ill-posedness at the boundary and hence complicates the analysis of fluid systems. This apparent discontinuity in the velocity field next to a solid surface (wall) can represent the existence of a very thin sheared zone with much smaller viscosity than the bulk (see Fig. 1).

In flow of entangled polymers, the wall slip occurs within the first layer of macromolecules adsorbed at the wall [see Figs. 1(c)–1(e)]. If the macromolecules are adsorbed to the surface, some parts of the chain are bound to the substrate along their backbone, and other chain sections can form loops and tails. These adsorbed chains are further entangled with chains in the bulk again [see Fig. 1(c)]. Under fast flow at a high Weissenberg number ($Wi = \tau\dot{\gamma}$, where τ is the characteristic relaxation time of polymeric fluid and $\dot{\gamma}$ is the imposed shear rate), the following possibilities exist: (i) flow induced stretching of adsorbed chains, leading to interfacial chain disentanglement of the strongly adsorbed chains from bulk chains [referred to as cohesive slip as shown in Fig. 1(d)],^{42,43} or (ii) detachment/desorption of the chains from the wall, leading directly to adhesive slip [as shown in Fig. 1(e)]. Typically, a slip layer is formed by a depletion of polymer chains (lubrication mechanism) during the desorption process when low surface energy coatings (such as fluoropolymers) are deposited on the wall surface.^{44–50} Over the last decade, several studies have been performed based on either near field laser velocimetry or particle tracking velocimetry (PTV) to characterize the wall slip during flow on solid substrates.^{51–60} Relevant parameters such as velocity at the wall (v_s) and extrapolation slip length $b = \frac{v_s}{dv/dz}$ can be extracted, where $\frac{dv}{dz}$ is the velocity gradient in the vicinity of the wall and z is the normal at the wall inwards to the fluid. Despite this large body of work based on velocimetry techniques, it is challenging to gain molecular insights into the nature of slip and understand its dependence on the wall properties.^{23,61}

Given the recent progress in biomicrofluidics, it is now possible to directly visualize the DNA conformation in different flow conditions by manipulating DNA molecules at micro-scale devices.^{2,62,63,76} For instance, we have recently integrated a commercial rheometer with a confocal fluorescence microscope capable of capturing the conformation of individual DNAs during

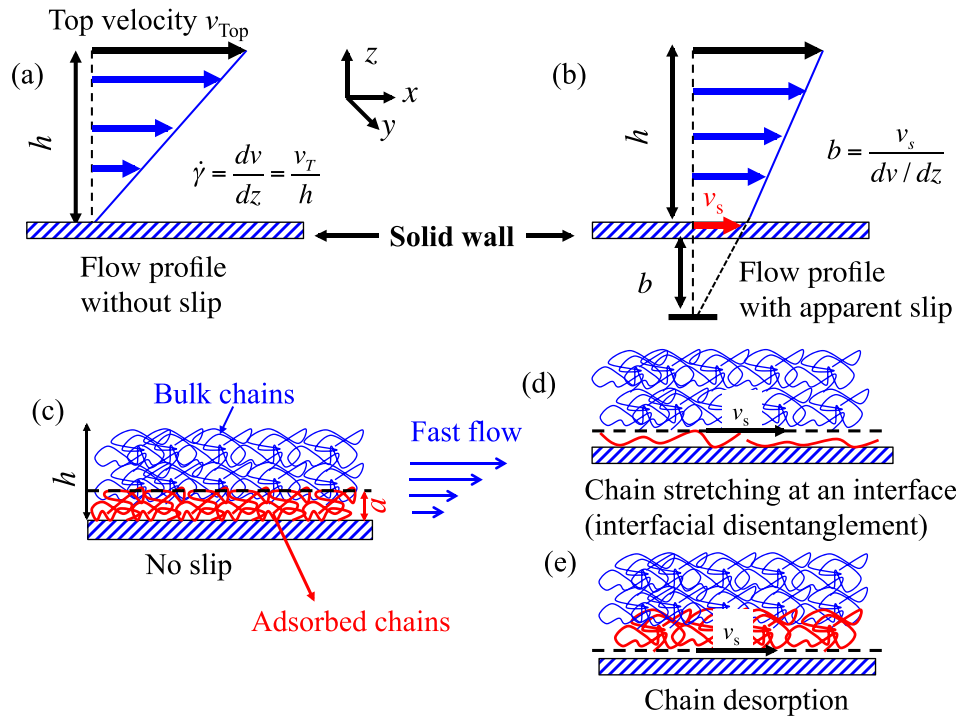


FIG. 1. Schematic of velocity profiles in the presence of external flow (with top velocity, v_{Top}) with (a) no-slip boundary condition and (b) slip boundary condition. The definition of the shear rate ($\dot{\gamma} = dV/dz$) and slip length (b) characterizes the flow gradient and the degree of boundary slip across the gap (h), respectively. (c) The schematic description of entangled polymer chains in the absence of slip, suggesting that polymeric chains are coiled. The molecular description of the slip mechanism when (d) flow-induced chain stretching (referred as to interfacial disentanglement) or (e) the chain desorption process occurs on a solid wall (during fast flow).

slip on an APTES-treated surface (with a strong interaction with DNA) in shear flow.⁶⁴ We showed that flow induced stretching of adsorbed chains (referred to as an interfacial disentanglement) is the only mechanism of slip during shear flow against APTES-treated surfaces. How generic this slip mechanism is and whether there exists a different mechanism of slip for polymer solutions flowing on different surfaces remain an open question. Here, we report a direct characterization of the DNA conformations in both the channel and shear flow and extend the single molecule DNA measurements on three different glass surfaces (ranging from untreated glass to APTES and acrylate modified glasses with different interactions). We perform local measurements of the velocity profiles and chain conformations by using DNA tracer molecules for all three different surfaces during flow. Such a molecular approach by changing the boundary conditions (from a weak to strong surface) allows us to directly decipher the chain desorption mechanism for both untreated glass and acrylate-treated glass, in contrast to the flow induced chain stretching for APTES-treated glass. In the latter case, we demonstrate that stretching is significantly increased at the surface as a function of the shear rate compared to the weak surfaces (unmodified surface or acrylate-treated glass). Furthermore, we find that the distribution of chain extension is still broad at high flow rates (at high Wi) due to molecular individual response of chains close to the surface. Knowledge of this independently measurable molecular extensions and conformations near the surface then allows us to develop a more realistic theory and quantitatively predict the molecular process of cohesive or adhesive slip in entangled polymer solutions.

II. EXPERIMENTAL METHODS

A. Preparation of DNA solution

To study the wall slip during shear or channel flow at the molecular level, we have prepared a solution of highly purified calf thymus DNA (molecular weight $\approx 5.0 \times 10^7$ g/mol or

75 kilo basepairs; used as received from USB Co.) in which a small fraction (0.07%) of the same DNA molecules is fluorescently labeled. Calf thymus DNA is dissolved in a TRIS buffer (10 mM Tris-HCl + 2 mM EDTA + 10 mM NaCl, pH = 8) at a concentration of 10 mg/ml to prepare well-entangled solution (the level of entanglement is $Z = 55$). The unstained calf thymus DNA has a radius of gyration (R_g) of $0.7 \mu\text{m}$, a persistence length (l_p) of $0.050 \mu\text{m}$, a contour length of $25.5 \mu\text{m}$, and a critical overlap concentration of 0.062 mg/ml . The radius of gyration has been calculated based on $R_g = 2l_p(aN/(12l_p))^\nu$, with $a = 0.34 \text{ nm}$ being the length of a base-pair, $N = 7.5 \times 10^4$ is the number of basepairs, and $\nu = 0.5$ for a theta solvent. It should be noted that most of the double-stranded DNAs used as model polymers (such as a λ -DNA; 48.5 kbp) do not display ideal scaling behavior and exist in the middle of the transition from a Gaussian to a swollen coil. Therefore, the power-law exponent of the end-to-end distance (ν) can be varied between 0.5 (corresponds to a Gaussian coil) and 0.588 (corresponds to a swollen chain).⁶⁵ The radius of gyration R_g of our DNA can be around $0.9 \mu\text{m}$ if we assume that $\nu = 0.57$. To image the tracer DNA molecules and capture the polymer conformation, the same calf thymus DNA is fluorescently labeled with YOYO-1 intercalating dye (Invitrogen) with a dye to base pair (bp) ratio of 1 to 5 and added to unstained DNA solution at a concentration of 0.1% using the same procedure as previously reported.⁶⁴ In addition, 0.3% v/v of β -mercaptoethanol was added to buffer solution to reduce photo bleaching. Previous work has shown that the contour length of stained DNA can increase by 38% at a dye/base pair ratio of 1:4.⁶⁶ Typically, it is assumed that the contour length of fluorescently labeled DNA increases linearly with an increasing staining ratio. In this work, we assume that the length of stained DNA is increased by 30% at a staining ratio of 1 YOYO-1 per 5 DNA base pairs. In this work, the visual length of fluorescently labeled DNA is divided by the (theoretical) stained contour length ($L_C = 33 \mu\text{m}$) to calculate the fractional extension during flow.

B. Microchannel fabrication

The microchannel with a rectangular cross section (width $w = 1 \text{ mm}$, length $l = 20 \text{ mm}$, and height $h = 80 \mu\text{m}$) is directly made on a methacrylate substrate using a high precision CNC micro-milling machine (Aerotech) as shown in Fig. S1 in the [supplementary material](#). To fabricate microfluidic devices in transparent polymethyl methacrylate (PMMA) sheets, end mills (Performance Micro Tool) of 1.5 mm , $508 \mu\text{m}$, and $127 \mu\text{m}$ have been selected and used to mill the inlet/outlet port. The micro-milled channel is then sealed by gluing a cover slip (either modified or un-modified) glass. The microchannel has been made to be wide so that sidewall flow effects can be minimized during microscopic measurements. Next, push-in gas tight connectors (Festo) have been glued to the top side of the chip for the inlet and outlet ports. To inject polymeric liquid through our microfluidic device via plastic tubing (outer diameter, OD = 3.175 mm), we have used a syringe pump (Pico Plus, Harvard Apparatus) with a 1 ml Hamilton Gastight Syringe (Inner Diameter, ID = 4.61 mm). This set-up is capable of producing flow rates between $0.16 \mu\text{l/h}$ and $2637 \mu\text{l/h}$. This microfluidics setup allows imaging at various heights, which can be used to generate velocity profiles from the bottom up to the middle of the channel in order to study the molecular response of DNA when interfacial slip occurs during flow [see Fig. 2(a)]. Flow in the rectangular micro-channel is induced at a fixed volumetric flow rate Q , where the shear rate on the fluid is approximately $\dot{\gamma} = \frac{2Q}{wh^2}$.⁶⁷ In all flow measurements, a constant flow rate has been imposed at room temperature ($T = 23 \pm 2^\circ\text{C}$) to reach steady-state flow (it took around 15 min to reach a steady-state in each measurement) without any detectable pulsation in the syringe pump.

C. Surface modification

To assess the role of surface conditions (with strong and weak interactions) on the slip phenomenon, either regular or chemically modified coverslip glasses (Fischer Scientific Inc., thickness = $0.15\text{--}0.16 \text{ mm}$ and local roughness $< 2 \text{ nm}$ from atomic force microscopy) have been assembled at the lower boundary of fluidic geometry (see Fig. 2). In channel flow experiments, the bottom walls of the microchannels consist of either a regular or (chemically) modified glass.

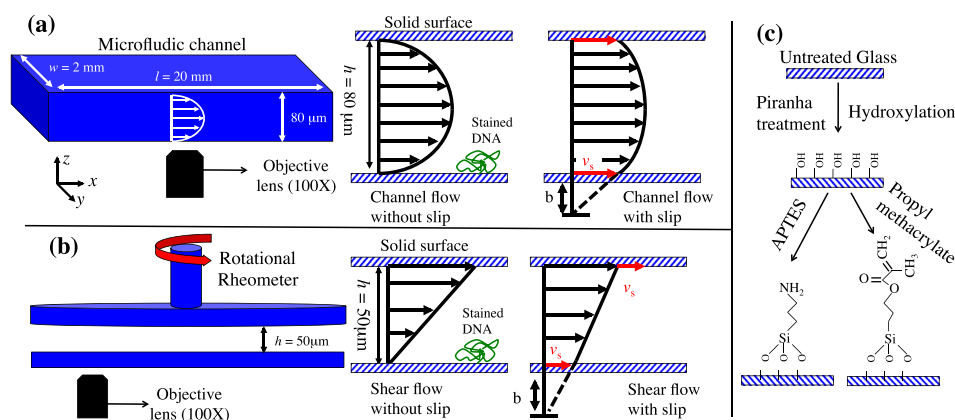


FIG. 2. Schematic figures: (a) a microfluidic channel and (b) a plate-plate rheometer with a transparent (regular or treated) plate and optics connected via an adjustable arm to the confocal scanner. The point of visualization was at the middle of the channel (at $w \approx 1$ and 10 mm from the entrance of the microchannel in channel flow). In the shear setup, DNA visualization was taken at 3 mm from the meniscus of the sample. (c) The procedure of surface modification of cover slip glasses with 3-aminopropyltriethoxysilane (APTES) and 3-(Trimethoxysilyl)propyl methacrylate (MA) after cleaning and activating the surface with a Piranha treatment.

The unmodified glass slides are cleaned with either ethanol or a Piranha solution (98% H_2SO_4 :30% H_2O_2 aqueous solution; ratio, 7:3 by mass), but these cleaning methods did not give systematic differences in the slip behavior of DNA solution. In shear experiments, we use a commercial rheometer with a parallel plate geometry (radius of the plate, $R = 12.5$ mm), where the bottom plate is a glass slide and the upper plate is a standard stainless steel plate. In shear experiments, the gap is set to $50 \mu\text{m}$, and the shear flow is provided by moving the top plate. Chemically grafted surfaces are obtained by coating the glass with either 3-aminopropyltriethoxysilane (APTES) or 3-(trimethoxysilyl)propyl methacrylate (MA) monolayers of silanes, as shown in Fig. 2(c). Due to APTES-functionalization of glass substrates, the surfaces (walls) have positive charges which provide a strong interaction with negatively charged DNA molecules.⁶⁸ However, both silicate glasses and PMMA surfaces immersed in aqueous solutions can acquire a negative surface charge.^{69,70} Therefore, they cannot interact very strongly with negatively charged DNA molecules due to electrostatic repulsion. Therefore, these surfaces cannot provide a strong interaction with negatively charged DNA molecules and will be served as weak surfaces in our work. Note that it has been demonstrated by molecular dynamics simulations that DNA can still bind to a (a negatively charged) silica surface effectively and the repulsion between silica and DNA can be weak due to the screening effect of the counterions near both surfaces.⁷¹ Furthermore, the DNA binding to silica nanoparticles also has been detected experimentally in a salt-free solution at $\text{pH} = 7$.⁷² The details of surface modification are described in the [supplementary material](#).

D. Velocimetry setup and DNA visualization

To visualize the conformation of DNAs during flow, the flow apparatus is assembled on a confocal microscope (equipped with a 100×1.45 numerical aperture oil-immersion objective lens). A confocal microscope system consisting of an Olympus IX-81 inverted microscope equipped with the Yokogawa CSU-22 high-speed confocal spinning disk and a Hamamatsu EMCCD camera (with 4×4 binning) has been used to take two dimensional images in the flow velocity direction (at a frame rate of 35 frames per second) at equal depth across the sample thickness. The field of view is about $75 \times 75 \mu\text{m}^2$ (with a resolution of $0.3 \mu\text{m}/\text{pixel}$). In shear experiments, imaging is performed at a sufficient distance of 3 mm from the edge, and all apparent shear rate values are estimated by $\dot{\gamma} = \Omega R/H$, where Ω is the imposed angular velocity at $R=9.5$ mm. A homemade microscope stage with three adjustable screws has been designed and assembled into an inverted microscope to ensure the alignment between the top and bottom plates (with a precision in the gap separation of about $\pm 4 \mu\text{m}$). This setup has been

previously employed to precisely conduct microscopic visualization for the confocal-rheoscopic study of solutions in the micron-scale gap.^{59,64} In channel flow, imaging is captured at a sufficient distance ($w \approx 0.5$ mm) from the microchannel sidewalls and in the middle of the channel ($l = 10$ mm) far from the inlet or outlet of the microfluidic device. Samples are sheared or flowed well into the steady state as confirmed by the velocity-time data for all results presented here. The spatial filtering of the pinhole apertures gives confocal increased lateral and axial resolution and enables thin focus plains to be attained. In our confocal setup, the diameter of the pinholes is $50 \mu\text{m}$, and the lateral resolution, axial resolution, and optical slice thickness are approximately 0.2, 0.5, and $0.8 \mu\text{m}$, respectively. Imaging of DNA molecules has been done by using an EMCCD camera (Hamamatsu) coupled with a confocal microscope. Stained DNA molecules are excited by a 491 nm laser line within our confocal setup. The velocity profiles were measured by tracking a strained DNA, a technique which has been reported before.⁶⁴ Typical error bars in the measured velocity are about 7%, which was achieved by keeping track of sufficiently large displacements of the stained DNA molecules.

E. Rheometric measurements

Before microscopic conformation measurements in our flow devices, the DNA solution is subjected to a series of rheological characterization. Macroscopic rheology data are obtained using a rheometer (Bohlin CVOR) with either a stainless steel cone-plate ($R = 12.5$ mm and cone angle $\theta = 4^\circ$) or a stainless steel parallel-plate geometry ($R = 12.5$ mm) at room temperature [as shown in Figs. 3(a) and 3(b)]. The smooth stainless steel surfaces are cleaned with acetone and ethanol before each shear experiment. A solvent trap has been employed to minimize the sample evaporation during shear measurements. First, the linear viscoelastic properties of DNA solution have been determined from small amplitude oscillatory shear (SAOS). Figure 3(a) displays the dynamic storage (G') and loss moduli (G'') of DNA solution as a function of frequency (ω) using a strain amplitude of 5%. A terminal relaxation time ($\tau = 14.5$ s) is estimated from the crossover frequency [$\omega = 1/\tau$, where $G' = G''$ as shown in Fig. 3(a)]. The elastic plateau modulus of DNA solution ($G_{pl} = 27$ Pa) has been calculated from the same SAOS test corresponding to the entanglement molecular weight $M_e = 0.91 \times 10^6$ g/mol (according to $M_e(C) = CRT/G_{pl}(C)$, where C is the concentration, R is the gas constant, and T is the temperature). The number of entanglements per chain Z can be estimated to be around 55 according to $Z = M_w/M_e(C)$, where M_w is the molecular weight of the parent DNA. Steady shear rheology is performed using a Bohlin rheometer at apparent shear rates ($\dot{\gamma}$) ranging from 0.001 s^{-1} to 100 s^{-1} in a rate controlled mode as shown in Fig. 3(b). Our DNA solution exhibits shear thinning, and the flow curve can be fitted quite well by the Carreau model as given below:

$$\eta - \eta_\infty = (\eta_0 - \eta_\infty) \left[1 + (\tau_C \dot{\gamma})^2 \right]^{\frac{n-1}{2}}. \quad (1)$$

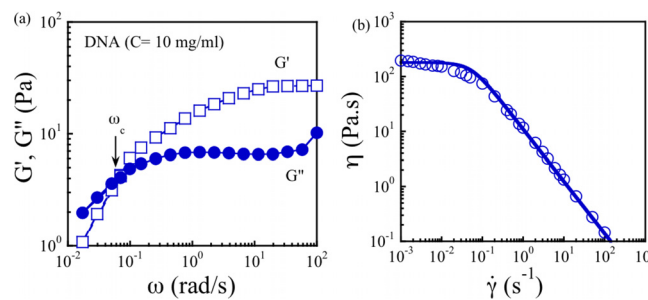


FIG. 3. Fluid rheological characterization using a commercially available macroscopic rheometer (Bohlin). (a) Frequency dependence of the storage moduli (G') and the loss moduli (G'') for DNA solution (with $C = 10$ mg/ml) at room temperature. The shear viscosity of DNA solution versus shear rate relation at the steady state measured (in the rate controlled mode) using a Bohlin rheometer (equipped with a standard stainless steel cone-plate geometry). The solid line represents the best fit to the DNA viscosity data using the Carreau model [see Eq. (1) in the text].

Here, η is the viscosity, η_0 is the zero-shear viscosity, η_∞ is the infinite shear viscosity (close to solvent viscosity, 0.001 Pa s), n is the power-law index, and τ_C is the estimated relaxation time (close to the reciprocal characteristic shear rate $\dot{\gamma}_C$ for the onset of shear-thinning). The characteristic relaxation time based on the Carreau model ($\tau_C = 19$ s) is close to the estimated relaxation time from the frequency sweep test [in Fig. 3(a)]. It should be noted that here we use $\tau = 14.5$ s (obtained from the SAOS test) to calculate the imposed Wi .

III. RESULTS AND DISCUSSION

First, we perform local velocity measurements at low flow rates ($Wi < 1.0$), where DNA solution behaves like a simple (Newtonian) fluid to check the accuracy of our micro-channel measurements. At a low flow rate ($Wi = 0.14$), the typical parabolic velocity profile with no slip has been obtained for the APTES-treated surface [as shown in Fig. 4(a)]. As we expected, conformational measurements show that all polymer chains are coiled (or unperturbed) when $Wi < 1.0$, as the parabolic flow obtained [see Fig. 4(b)]. However, we observe significant slip close to the wall of regular glass at low Wi ($Wi = 0.2$). In this case, DNA molecules are still coiled with significant slip velocity at the surface [see Fig. 4(c)]. This originates from the weak interaction between the adsorbed chains and the wall, leading to produce significant slip even in the Newtonian regime as reported before.⁷³

Next, we explore the role of the surface on wall slip and conformation of adsorbed chains when $Wi > 1.0$. Figures 5(a)–5(d) show that significant wall slip occurs across the height of the channel at $Wi = 5.6$ for both APTES-treated and untreated surfaces. At $Wi = 5.6$, the localized velocity profile is plug flow for the untreated surface, as compared to APTES-treated surfaces. This is actually due to the stronger interaction of adsorbed chains with the APTES-treated surface compared to regular glass. Microscopic investigations have shown that surface properties play a significant role in the conformation of DNA in the slip regime [see Fig. 5(b)]. Polymeric chains at the surface of the APTES-treated surface are partially stretched at high Wi (around 5); however, other chains remain coiled across the channel height. Conversely, for the untreated surface, polymeric chains are desorbed, and a thin layer of water is present at the surface, which induces an effective slip of polymer during flow. At a higher flow rate ($Wi = 22.6$), both velocity profiles are similar, and they show plug flows [see Fig. 5(c)]. However, flow-induced chain stretching occurs close to the wall of the APTES-treated surface, compared to the desorption process in regular (untreated) glasses.

To achieve a more quantitative comparison between two surfaces, we have analyzed the extension probability distributions (in the slip layer) during steady flow at $Wi = 5.6$ and 22.6.

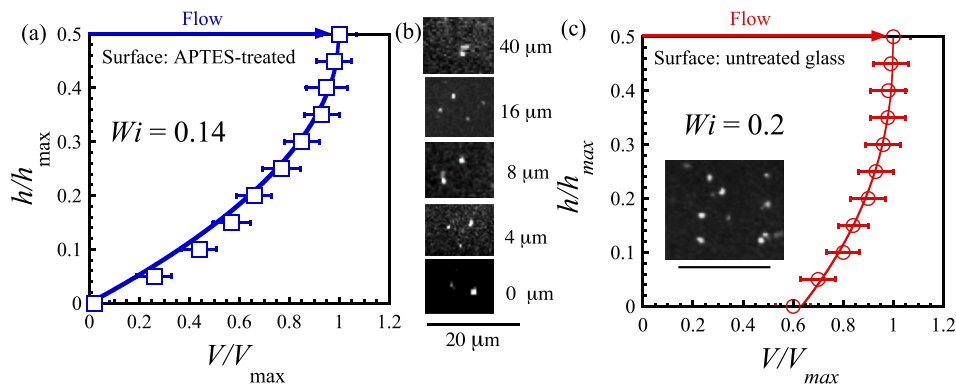


FIG. 4. (a) A parabolic channel flow at low $Wi = 0.14$ obtained for APTES-treated surfaces by microscopic measurements using a CFM coupled to a rectangular micro-channel ($V_{max} = 0.56 \mu\text{m/s}$). The solid line represents the fitting of the profile by fitting the Hagen-Poiseuille law. (b) DNA images during steady flow at different heights of the channel (from the surface to the middle of the channel) at $Wi = 0.14$. The error bars represent the percent deviation in each dataset. (c) A flow profile with apparent slip for untreated (regular) glasses at $Wi = 0.2$ ($V_{max} = 0.69 \mu\text{m/s}$). The solid line represents the fitting of the velocity profile by the power-law fit. The error bars correspond to the standard deviation of the measurements.

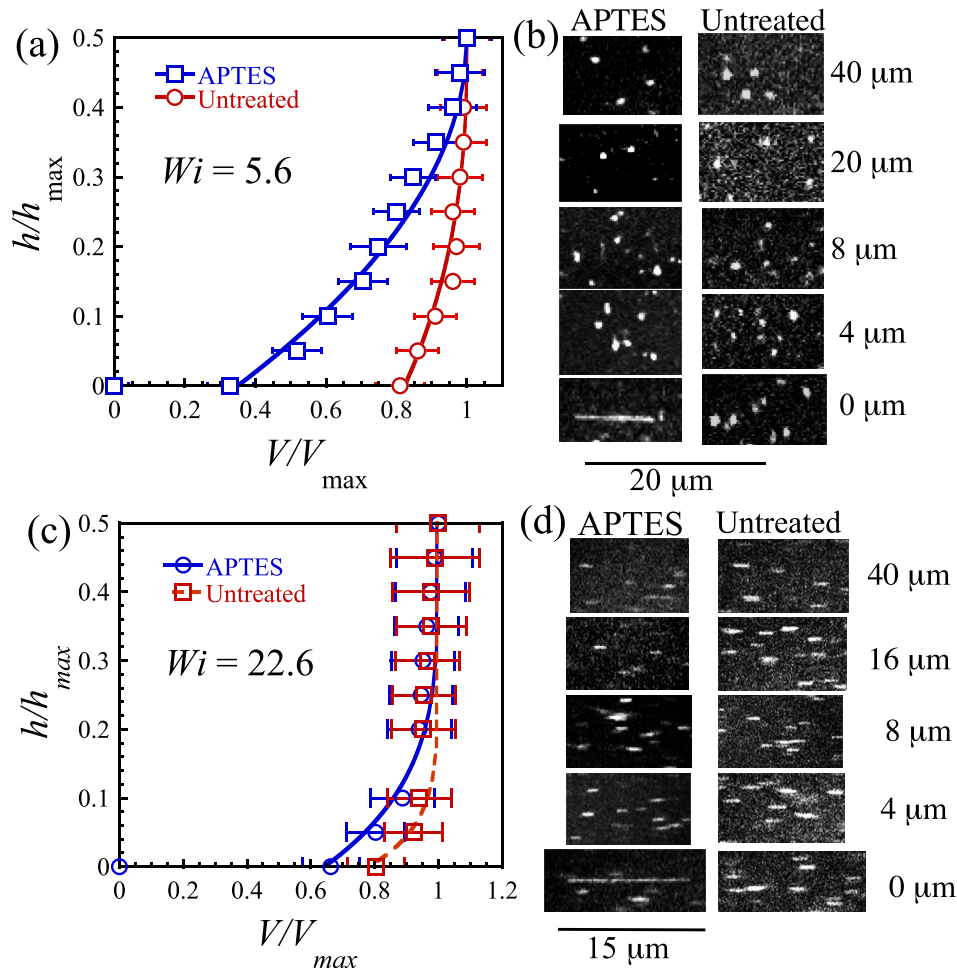


FIG. 5. (a) Velocity profiles obtained in a rectangular microchannel for APTES-treated and untreated substrates at $Wi = 5.6$ ($V_{max} = 19.5$ and $19.8 \mu\text{m/s}$ for APTES-treated and untreated surfaces, respectively). (b) The molecular conformation of DNA across the channel height during steady flow for two surfaces. (c) Velocity profile and (d) conformational measurements for APTES-treated and untreated substrates at $Wi = 22.6$ ($V_{max} = 83$ and $88 \mu\text{m/s}$ for APTES-treated and untreated surfaces, respectively). The solid and dashed lines represent the fitting of the velocity profiles by the power-law fit.

Figure 6(a) displays the probability distributions of polymer extension for the APTES-treated surface at $Wi = 5.6$ categorized in the mobile and immobile regions. It is observed that the immobile DNA molecules at the surface have a higher level of stretch, in contrast to the mobile chains that remain coiled. As can be seen from Fig. 6(b), all DNA chains at regular glass appear in a much more coiled conformation than those located on the APTES surface. This feature is consistent with the proposed chain desorption mechanism for wall slip in regular glasses, compared to the flow-induced chain stretching mechanism (can be related to the interfacial disentanglement process) on APTES-treated surfaces. It is important to emphasize that it is almost impossible to image only adsorbed chains in our single molecule experiments due to spatial resolution limitations in the height direction. Therefore, it is plausible that the mobile chains (corresponding to the coiled polymers) can be slightly above the stationary surface and are not adsorbed chains. This is also consistent with the theoretical picture of a coil-stretch transition of the adsorbed chains occurring at the first monolayer of adsorbed polymer chains on the surface, and nearest neighbours in the next layer remain in the coiled conformation and entangled with other bulk chains.^{23,43,74} In addition, we find that the average conformation of immobile chains reaches a higher level of molecular extension at $Wi = 22.6$, compared to $Wi = 5.6$ on APTES surfaces. At the same $Wi = 22.6$ on a regular glass, the DNA molecules still contain a signature of the preponderance of the coil-sized chain configurations during flow. Furthermore,

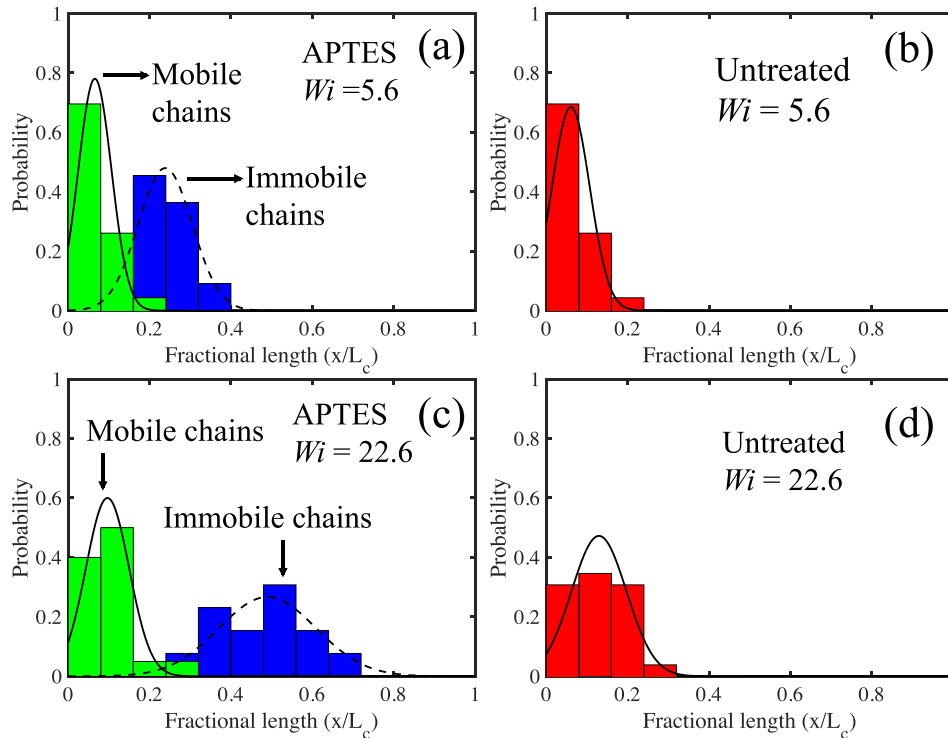


FIG. 6. (a)–(d) Extension probability distributions for two surfaces (columns) and flow rates (rows). DNA images during steady flow at $Wi = 5.6$ and 22.6 are shown. In each single-molecule experiment, the probability distribution is obtained from ≈ 30 individual molecules. Note that the solid and dashed lines are the normal distribution fit to the data shown solely to guide the reader's eye.

Figs. 6(a)–6(d) show that flow rates with higher Wi tend to broaden the size distribution considerably (in particular for the immobile region on APTES surfaces). These data exhibit that molecular individualism has been presented in our single molecule experiment at the interface between adsorbed chains and the solid substrate. Similar broad distributions have also been observed by single molecule experiments in both shear and extensional flows of polymer solutions at fast flow rates ($Wi > 1.0$) for both λ - and T4- DNA molecules.^{75–77} It should be noted that both λ - and T4- DNA molecules have a narrow size distribution, compared to our calf thymus DNA molecules. Recently, Hsiao *et al.*⁷⁷ reported that semi-dilute λ -DNA solutions can display a much broader distribution compared to dilute solutions due to intermolecular interactions.

Going further, we also perform local velocity measurements in a micron-scale shear cell ($h \approx 50 \mu\text{m}$), for which stress is uniform across the gap for APTES and MA-treated glasses. Figure 7(a) shows the stress overshoot characteristics at a shear rate of 0.5 s^{-1} ($Wi = 7.3$) for both treated surfaces. It is clear that stress overshoot is stronger for the APTES-treated surface, compared to the MA-treated surface. Figure 7(b) displays the velocity profiles from the shear measurements for a given shear rate ($\dot{\gamma} = 0.5 \text{ s}^{-1}$). Linear velocity profiles with strong slip are obtained only on the bottom surfaces (for both APTES- and MA-treated glasses). Next, the bulk shear rates are estimated from the velocity profile using ordinary least squares regression. We find that the bulk shear rate of the MA-treated surface ($\dot{\gamma}_b \approx 0.02 \text{ s}^{-1}$) is significantly lower than the bulk shear rate of the APTES-treated surface ($\dot{\gamma}_b \approx 0.25 \text{ s}^{-1}$). We now investigate the microscopic origin of this slip behaviour by analyzing the probability distribution of fractional extension at APTES- and MA-treated surfaces [see Figs. 7(c) and 7(d)], in a fashion similar to the previous case (channel flow on treated and untreated glass). Our data [from Fig. 7(c)] show that the probability distribution function of the normalized stretch length of DNA molecules can still be classified into two separate regions of mobile and immobile chains at APTES-treated surfaces during slip (similar to channel flow). The distribution corresponding to mobile

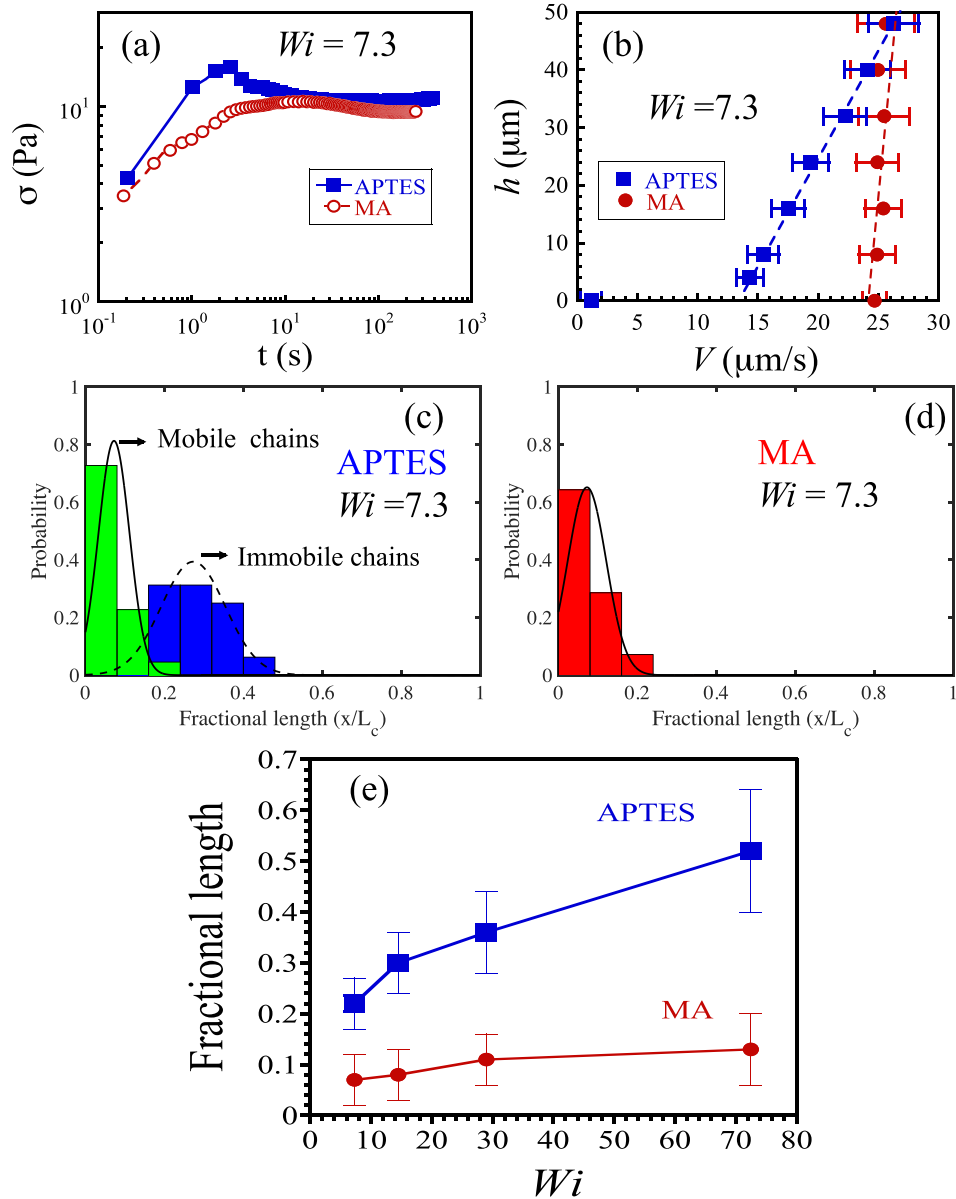


FIG. 7. (a) Shear stress growth at a startup shear rate of 0.5 s^{-1} on APTES-treated and MA-treated surfaces ($\Omega = 2.6 \times 10^{-3} \text{ rad/s}$). (b) Corresponding local velocity profiles obtained using the parallel disk geometry at a shear rate of 0.5 s^{-1} (in the steady state at $t = 100 \text{ s}$). Note that the top surface is stainless steel which has a stronger interaction with DNA solution. No detectable slip has been observed on the top plate at this shear rate. The estimated bulk shear rates from velocity profiles are 0.25 and 0.02 s^{-1} for APTES- and MA-treated surfaces, respectively. The probability distribution of chain extension for (c) APTES- and (d) MA-treated glass at $Wi = 7.3$. In each single-molecule experiment, the probability distribution is obtained from ≈ 30 individual molecules. Note that the solid and dashed lines are the normal distribution fit to the data shown solely to guide the reader's eye. (e) The mean fractional length is plotted against Wi for both surfaces.

chains is mostly coiled (with the majority of the normalized extensions ranging from 0.02 to 0.17) as shown in Fig. 7(c). However, the distribution of normalized stretch lengths for immobile chains has a higher level of stretch ranging from 0.2 to 0.5. Here, we also observe a broad distribution in the immobile adsorbed chains where a flow-induced chain stretching transition occurs on them. The broadness of the distribution may account for the effect of calf thymus DNA polydispersity. However, previous works showed that the similar broadness of the distribution can be occurred at high Wi ($Wi > 1.0$) in shear flow of semi-dilute and entangled λ -DNA solutions (with a narrow size distribution).^{75,78} In particular, it has been also demonstrated that

the probability distribution broadens with the imposed strain in both start-up shear and extensional flow measurements, indicating the presence of molecular individualism.^{77,78} For the MA-treated surface (at same Wi), the majority of DNA molecules are found at the coiled conformation [see Fig. 7(d)]. For the MA-treated surface, we can conclude that the chain desorption (detachment) governs the interfacial slip during shear flow. Figure 7(e) displays the mean extension of chains at the surface as a function of $\dot{\gamma}$ for both APTES- and MA-treated surfaces. The results for the APTES-treated surface (filled squares) indicate that the mean extension of DNA increases gradually with a shear rate. The mean fractional extension approaches around 0.7 at $\dot{\gamma} = 5.0 \text{ s}^{-1}$ ($Wi = 72.5$). However, on the MA-treated surface, DNA chains are still coiled (at the same Wi), suggesting that chain desorption results wall slip during shear on weak surfaces. This directly indicates that the molecular mechanism of slip is very sensitive to the surface conditions.

To better quantify the experimental data obtained during shear or channel flow, the slip velocity (v_s) is also plotted versus Wi on different surfaces (in Fig. 8). First, we find that the slip velocity increases linearly with imposed Wi (when $Wi > 1.0$), and slip velocities on different surfaces are almost overlapped in this regime. Therefore, there is no large surface effect on slip velocity for DNA solution during flow on regular glass and APTES- and MA-treated surfaces. However, at low Wi , the slip velocity still occurs during flow on weak surfaces (both the MA-treated surface and regular glass), compared to the APTES-treated surface (with no slip condition). In the absence of slip, polymer chains close to the interface move with a very small velocity approximated as $v_{ns} \approx R_g \times \dot{\gamma}$, where R_g is the radius of gyration (R_g of DNA is around $0.7 \mu\text{m}$) (see the open square and triangles in the lower branch of Fig. 8 at $Wi < 1.0$). This figure shows that significant slip can still occur on weak surfaces (regular glass and MA-treated surfaces) even at low Wi ($Wi < 1.0$). This result suggests that critical Wi (or shear stress) for wall slip by the chain desorption mechanism is lower than the interfacial chain disentanglement mechanism. Previous studies based on capillary flow also showed that critical stress for slip is very sensitive to the coating of capillary die and reported that critical stress for wall slip is lower in the case of weak surfaces.^{73,79} Previous reports showed that the effectiveness of a simple coating with a fluoropolymer or soap solution around the die plays a role in eliminating the shark-skin fracture during extrusion of polymeric liquids.^{80–82} Lack of chain stretching on weak surfaces can explain this phenomenon, as we have confirmed it by our single-molecule experiments on the weak surfaces.

IV. CONCLUSIONS

In this work, we have performed an extensive single-molecule investigation on different wall surfaces to provide new insights into the mechanism of interfacial slip. To elucidate the

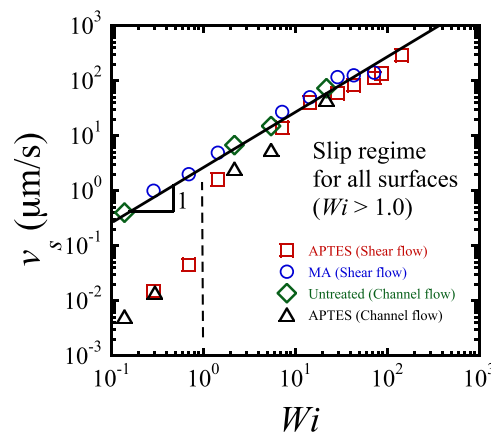


FIG. 8. Slip velocity of DNA solution versus Wi during shear or channel flow on three different surfaces ranging from untreated glass to APTES- and MA- treated surfaces. When $Wi > 1.0$, all surfaces show a similar apparent slip velocity as a function of Wi . In the absence of slip (at $Wi < 1.0$ for the APTES-treated surface), polymer chains close to the interface move with a very small velocity approximated as $v_{ns} \approx R_g \times \dot{\gamma}$, where R_g is the radius of gyration (the R_g of DNA is around $0.7 \mu\text{m}$).

microscopic origin of wall slip on different surface conditions (with either a weak or strong interaction), a confocal microscope has been integrated with a microscale shear cell (or microchannel) for DNA imaging across the sample thickness (from the surface/interface to bulk). We have employed fluorescently labeled DNA molecules to capture the conformational changes of adsorbed polymer flowing on solid substrates. Depending on surface conditions, we find that two distinctly different molecular processes can induce interfacial slip for the same DNA solution. In channel flow, we confirm a parabolic flow across the channel height with negligible slip for APTES-treated glass (with a strong interaction with DNA chains) at low Wi ($Wi < 1$). All DNA molecules remain coiled during flow at low Wi . While Wi increases, a coil-stretch transition occurs only for the adsorbed chains during flow, resulting in wall slip. Compared to the APTES-treated surface, we have shown that chain desorption (or chain detachment) process occurs for the untreated glass or MA-treated surface, resulting in formation of a layer of desorbed chains during shear and flow. This chain desorption mechanism is confirmed by the lack of chain stretching for DNA chains at the interface. There is increased interest in DNA molecular behaviour near solid surfaces in micro/nanoscale geometries, as well as DNA stretching and deposition onto a solid substrate.^{41,83} We anticipate that local polymer conformation near the interface and bulk can play a crucial role in the fluid dynamics and nonlinear rheological properties of polymer solutions.⁸⁴ We believe that these single molecule experiments can provide more insights into a realistic theoretical picture of polymer flow (with different architectures and levels of entanglement) near solid surfaces (with different surface properties), which allows us to optimize these stretching processes more efficiently.^{2,41,83}

SUPPLEMENTARY MATERIALS

See [supplementary material](#) for the details of surface modification, DNA solution preparation, microchannel fabrication, and alignment of (low gap) the rheometer.

ACKNOWLEDGMENTS

We gratefully thank financial support from European Research Council (ERC) under the European Union's Seventh Framework Programme (FP/2007–2013)/ERC Grant, Agreement No. 337820 (to P.E.B.). In addition, the authors thank S. Sachdev, D. Kawale, A. Muralidharan, and L. Rems for their insightful comments on several subjects.

- ¹P. Nghe, E. Terriac, M. Schneider, Z. Z. Li, M. Cloitre, B. Abecassis, and P. Tabeling, *Lab Chip* **11**, 788 (2011).
- ²L. Rems, D. Kawale, L. J. Lee, and P. E. Boukany, *Biomicrofluidics* **10**, 043403 (2016).
- ³S. Goldstein and A. R. C. G. Britain, *Modern Developments in Fluid Dynamics: An Account of Theory and Experiment Relating to Boundary Layers, Turbulent Motion and Wakes*, Oxford Engineering Science Series (The Clarendon Press, 1938).
- ⁴J. B. J. Koplik, *Annu. Rev. Fluid Mech.* **27**, 257 (1995).
- ⁵J. Atencia and D. J. Beebe, *Nature* **437**, 648 (2005).
- ⁶S. Granick, Y. Zhu, and H. Lee, *Nat. Mater.* **2**, 221 (2003).
- ⁷P. Joseph and P. Tabeling, *Phys. Rev. E* **71**, 035303 (2005).
- ⁸O. I. Vinogradova, K. Koynov, A. Best, and F. m c. Feuillebois, *Phys. Rev. Lett.* **102**, 118302 (2009).
- ⁹M. M. Denn, *Annu. Rev. Fluid Mech.* **33**, 265 (2001).
- ¹⁰V. Mhetar and L. A. Archer, *Macromolecules* **31**, 8607 (1998).
- ¹¹P. E. Boukany, P. Tapadia, and S.-Q. Wang, *J. Rheol.* **50**, 641 (2006).
- ¹²S. G. Hatzikiriakos, *Prog. Polym. Sci.* **37**, 624 (2012), topical Issue on Polymer Physics.
- ¹³T. Himmel and M. H. Wagner, *J. Rheol.* **57**, 1773 (2013).
- ¹⁴S. P. Meeker, R. T. Bonnecaze, and M. Cloitre, *Phys. Rev. Lett.* **92**, 198302 (2004).
- ¹⁵M. P. Lettinga and S. Manneville, *Phys. Rev. Lett.* **103**, 248302 (2009).
- ¹⁶S. Manneville, A. Colin, G. Waton, and F. Schosseler, *Phys. Rev. E* **75**, 061502 (2007).
- ¹⁷P. E. Boukany and S.-Q. Wang, *Macromolecules* **41**, 1455 (2008).
- ¹⁸N. D. Denkov, V. Subramanian, D. Gurovich, and A. Lips, papers presented at the *5th European Conference on Foams, Emulsions, and Applications, {EUFOAM} 2004, University of Marne-la-Vallee, Champs sur Marne, France, 5–8 July 2004* [Colloids Surf. A: Physicochem. Eng. Aspects **263**, 129 (2005)].
- ¹⁹I. Cantat, *Phys. Fluids* **25**, 031303 (2013).
- ²⁰J. Paredes, N. Shahidzadeh, and D. Bonn, *Phys. Rev. E* **92**, 042313 (2015).
- ²¹J. Persello, A. Magnin, J. Chang, J. M. Piau, and B. Cabane, *J. Rheol.* **38**, 1845 (1994).
- ²²P. Ballesta, G. Petekidis, L. Isa, W. C. K. Poon, and R. Besseling, *J. Rheol.* **56**, 1005 (2012).
- ²³S. G. Hatzikiriakos, *Soft Matter* **11**, 7851 (2015).

- ²⁴R. I. Tanner, *Ind. Eng. Chem. Res.* **33**, 2434 (1994).
- ²⁵N. Willenbacher, H. Hanciogullari, and H. G. Wagner, *Chem. Eng. Technol.* **20**, 557 (1997).
- ²⁶L. De Vargas and O. Manero, *Polym. Eng. Sci.* **29**, 1232 (1989).
- ²⁷G. Chauveteau, M. Tirrell, and A. Omari, *J. Colloid Interface Sci.* **100**, 41 (1984).
- ²⁸A. Cuenca and H. Bodiguel, *Lab Chip* **12**, 1672 (2012).
- ²⁹A. Cuenca and H. Bodiguel, *Phys. Rev. Lett.* **110**, 108304 (2013).
- ³⁰D. Kawale, E. Marques, P. L. J. Zitha, M. T. Kreutzer, W. R. Rossen, and P. E. Boukany, *Soft Matter* **13**, 765 (2017).
- ³¹S. Hatzikiriakos and K. Migler, *Polymer Processing Instabilities: Understanding and Control*, Chemical Industries Series (Marcel Dekker, 2005).
- ³²J. Cayer-Barrioz, D. Mazuyer, A. Tonck, and E. Yamaguchi, *Tribol. Lett.* **32**, 81 (2008).
- ³³A. Dedinaite, *Soft Matter* **8**, 273 (2012).
- ³⁴H. Craighead, *Nature* **442**, 387 (2006).
- ³⁵J. M. Sidorova, N. Li, D. C. Schwartz, A. Folch, and R. J. Monnat, Jr., *Nat. Protocols* **4**, 849 (2009).
- ³⁶G.-L. He, R. Messina, H. Lowen, A. Kiriy, V. Bocharova, and M. Stamm, *Soft Matter* **5**, 3014 (2009).
- ³⁷G. Yu, A. Kushwaha, J. K. Lee, E. S. G. Shaqfeh, and Z. Bao, *ACS Nano* **5**, 275 (2011).
- ³⁸S.-Q. Wang and P. Drda, *Macromol. Chem. Phys.* **198**, 673 (1997).
- ³⁹J. Eijkel, *Lab Chip* **7**, 299 (2007).
- ⁴⁰A. Ajdari and L. Bocquet, *Phys. Rev. Lett.* **96**, 186102 (2006).
- ⁴¹P. J. Glazer, L. Bergen, L. Jennings, A. J. Houtepen, E. Mendes, and P. E. Boukany, *Small* **10**, 1729 (2014).
- ⁴²F. Brochard-Wyart, C. Gay, and P.-G. de Gennes, *Macromolecules* **29**, 377 (1996).
- ⁴³F. Brochard and P. G. D. Gennes, *Langmuir* **8**, 3033 (1992).
- ⁴⁴S. G. Hatzikiriakos and J. M. Dealy, *Int. Polym. Process.* **8**, 36 (1993).
- ⁴⁵N. Kissi, L. Léger, J.-M. Piau, and A. Mezghani, *J. Non-Newtonian Fluid Mech.* **52**, 249 (1994).
- ⁴⁶J. R. Barone and S.-Q. Wang, *J. Non-Newtonian Fluid Mech.* **91**, 31 (2000).
- ⁴⁷Y. Inn and S.-Q. Wang, *Phys. Rev. Lett.* **76**, 467 (1996).
- ⁴⁸D. A. Hill, T. Hasegawa, and M. M. Denn, *J. Rheol.* **34**, 891 (1990).
- ⁴⁹T. T. Dao and L. A. Archer, *Langmuir* **18**, 2616 (2002).
- ⁵⁰S. H. Anastasiadis and S. G. Hatzikiriakos, *J. Rheol.* **42**, 795 (1998).
- ⁵¹K. B. Migler, H. Hervet, and L. Leger, *Phys. Rev. Lett.* **70**, 287 (1993).
- ⁵²L. Leger, H. Hervet, G. Massey, and E. Durliat, *J. Phys.: Condens. Matter* **9**, 7719 (1997).
- ⁵³H. Münstedt, M. Schmidt, and E. Wassner, *J. Rheol.* **44**, 413 (2000).
- ⁵⁴P. E. Boukany and S.-Q. Wang, *Macromolecules* **42**(6), 2222–2228 (2009).
- ⁵⁵H. Kambara, S. Kashiwaya, H. Yaguchi, Y. Asano, Y. Tanaka, and Y. Maeno, *Phys. Rev. Lett.* **101**, 267003 (2008).
- ⁵⁶K. A. Hayes, M. R. Buckley, I. Cohen, and L. A. Archer, *Phys. Rev. Lett.* **101**, 218301 (2008).
- ⁵⁷S. M. Sabzevari, I. Cohen, and P. M. Wood-Adams, *Macromolecules* **47**, 3154 (2014).
- ⁵⁸S. M. Sabzevari, I. Cohen, and P. M. Wood-Adams, *Macromolecules* **47**, 8033 (2014).
- ⁵⁹P. E. Boukany, S.-Q. Wang, S. Ravindranath, and L. J. Lee, *Soft Matter* **11**, 8058 (2015).
- ⁶⁰M. Hénot, A. Chennevière, E. Drockenmuller, L. Léger, and F. Restagno, *Macromolecules* **50**, 5592 (2017).
- ⁶¹A. L. Yarin and M. D. Graham, *J. Rheol.* **42**, 1491 (1998).
- ⁶²X. Hu, P. E. Boukany, O. L. Hemminger, and L. J. Lee, *Macromol. Mater. Eng.* **296**, 308 (2011).
- ⁶³O. Hemminger, P. E. Boukany, S. Q. Wang, and L. J. Lee, *J. Non-Newtonian Fluids* **165**, 1613 (2010).
- ⁶⁴P. E. Boukany, O. Hemminger, S.-Q. Wang, and L. J. Lee, *Phys. Rev. Lett.* **105**, 027802 (2010).
- ⁶⁵D. R. Tree, A. Muralidhar, P. S. Doyle, and K. D. Dorfman, *Macromolecules* **46**, 8369 (2013).
- ⁶⁶B. Kundukad, J. Yan, and P. S. Doyle, *Soft Matter* **10**, 9721 (2014).
- ⁶⁷C. J. Pipe, T. S. Majmudar, and G. H. McKinley, *Rheol. Acta* **47**, 621 (2008).
- ⁶⁸J. Jing, J. Reed, J. Huang, X. Hu, V. Clarke, J. Edington, D. Housman, T. S. Anantharaman, E. J. Huff, B. Mishra, B. Porter, A. Shenker, E. Wolfson, C. Hiort, R. Kantor, C. Aston, and D. C. Schwartz, *Proc. Natl. Acad. Sci.* **95**, 8046 (1998).
- ⁶⁹B. J. Kirby and E. F. Hasselbrink, *Electrophoresis* **25**, 187 (2004).
- ⁷⁰B. J. Kirby and E. F. Hasselbrink, *Electrophoresis* **25**, 203 (2004).
- ⁷¹B. Shi, Y. K. Shin, A. A. Hassanali, and S. J. Singer, *J. Phys. Chem. B* **119**, 11030 (2015).
- ⁷²P. Mercier and R. Savoie, *Biospectroscopy* **3**, 299 (1997).
- ⁷³S. G. Hatzikiriakos and J. M. Dealy, *J. Rheol.* **35**, 497 (1991).
- ⁷⁴A. Adjari, F. Brochard-Wyart, P.-G. de Gennes, L. Leibler, J.-L. Viovy, and M. Rubinstein, *Phys. A: Stat. Mech. Appl.* **204**, 17–39 (1994).
- ⁷⁵R. E. Teixeira, A. K. Dambal, D. H. Richter, E. S. G. Shaqfeh, and S. Chu, *Macromolecules* **40**, 2461 (2007).
- ⁷⁶S. Sachdev, A. Muralidharan, and P. E. Boukany, *Macromolecules* **49**, 9578 (2016).
- ⁷⁷K.-W. Hsiao, C. Sasmal, J. R. Prakash, and C. M. Schroeder, *J. Rheol.* **61**, 151 (2017).
- ⁷⁸J. S. Hur, E. S. G. Shaqfeh, H. P. Babcock, D. E. Smith, and S. Chu, *J. Rheol.* **45**, 421 (2001).
- ⁷⁹X. Yang, S.-Q. Wang, A. Halasa, and H. Ishida, *Rheol. Acta* **37**, 415 (1998).
- ⁸⁰W. Y. Inn, J. R. Fischer, and T. M. Shaw, *Rheol. Acta* **37**, 573 (1998).
- ⁸¹K. B. Migler, C. Lavallée, M. P. Dillon, S. S. Woods, and C. L. Gettinger, *J. Rheol.* **45**, 565 (2001).
- ⁸²R. P. Rutgers and M. R. Mackley, *J. Non-Newtonian Fluid Mech.* **98**, 185 (2001).
- ⁸³J. J. Benitez, J. Topolancik, H. C. Tian, C. B. Wallin, D. R. Latulippe, K. Szeto, P. J. Murphy, B. R. Cipriany, S. L. Levy, P. D. Soloway, and H. G. Craighead, *Lab Chip* **12**, 4848 (2012).
- ⁸⁴P. E. Boukany and S.-Q. Wang, *J. Rheol.* **53**, 1425 (2009).